frontiers | Frontiers in Earth Science

TYPE Original Research
PUBLISHED 13 April 2023
DOI 10.3389/feart.2023.1188302

OPEN ACCESS

EDITED BY
Peng Tan,
CNPC Engineering Technology R&D Company Limited, China

REVIEWED BY
Wang Zepeng,
Henan Polytechnic University, China
Jianghui Ding,
CNPC Engineering Technology R&D Company Limited, China

*CORRESPONDENCE
Jingwei Zheng,
zhengjingwei@cqu.edu.cn
Saipeng Huang,
huangspcugb@hotmail.com

RECEIVED 17 March 2023
ACCEPTED 03 April 2023
PUBLISHED 13 April 2023

CITATION
Li C, Zheng J and Huang S (2023), The effects of supercritical CO_2 on the seepage characteristics and microstructure of water-bearing bituminous coal at *in-situ* stress conditions.
Front. Earth Sci. 11:1188302.
doi: 10.3389/feart.2023.1188302

The effects of supercritical CO_2 on the seepage characteristics and microstructure of water-bearing bituminous coal at *in-situ* stress conditions

Chengtian Li[1,2], Jingwei Zheng[1,2]* and Saipeng Huang[3,4]*

[1]State Key Laboratory of Coal Mine Disaster Dynamics and Control, Chongqing University, Chongqing, China, [2]School of Resources and Safety Engineering, Chongqing University, Chongqing, China, [3]Key Laboratory of Continental Shale Hydrocarbon Accumulation and Efficient Development, Ministry of Education, Northeast Petroleum University, Daqing, China, [4]Department de Mineralogia, Petrologia i Geologia Aplicada, Facultat de Ciències de la Terra, Universitat de Barcelona (UB), Barcelona, Spain

CO_2 geological storage (CGS) is considered to be an important technology for achieving carbon peak and carbon neutralization goals. Injecting CO_2 into deep unminable coal seams can achieve both CGS and enhance coalbed methane (ECBM) production. Therefore, the deep unminable coal seams are considered as promising geological reservoirs. CO_2 exists in a supercritical CO_2 ($ScCO_2$) when it was injected into deep unminable coal seams. The injection of $ScCO_2$ can induce changes in the seepage characteristics and microstructure of deep water-bearing coal seams. In this study, typical bituminous coal from Shenmu, Shanxi Province was used to investigate the effects of $ScCO_2$ on seepage characteristics, pore characteristics, and mineral composition through experiments such as seepage tests, low-temperature liquid nitrogen adsorption, and X-ray diffraction (XRD). The results indicate that $ScCO_2$ treatment of dry and saturated coal samples caused a significant increase in clay mineral content due to the dissolution of carbonates, leading to the conversion of adsorption pores to seepage pores and an improvement in seepage pore connectivity. Therefore, the Brunauer-Emmett-Teller (BET) specific surface area and pore volume of the two coal samples both decreased after $ScCO_2$ treatment. Moreover, the permeability of dry and saturated coal samples increased by 191.53% and 231.71% at 10 MPa effective stress respectively. In semi-saturated coal samples, a large amount of dolomite dissolved, leading to the precipitation of Ca^{2+} and CO_3^{2-} to form calcite. This caused pore throats to clog and macropores to divide. The results show that the pore volume and average pore size of coal samples decrease, while the specific surface area increases after $ScCO_2$ treatment, providing more space for gas adsorption. However, the pore changes also reduced the permeability of the coal samples by 32.21% and 7.72% at effective stresses of 3 MPa and 10 MPa, respectively. The results enhance our understanding of carbon sequestration through $ScCO_2$ injection into water-bearing bituminous coal seams.

KEYWORDS

bituminous coal, *in situ* stress, supercritical CO_2, seepage characteristics, pore characteristics, mineral composition

1 Introduction

Massive CO_2 emissions contribute to the global greenhouse effect, which in turn causes a series of climate catastrophes. Scholars worldwide have proposed many carbon reduction options in response (Liu et al., 2019; Li X. et al., 2022; Xu et al., 2022), including carbon geological storage (CGS), which has gained recognition as an effective way to achieve CO_2 sequestration and reduce greenhouse gas emissions (Wang Y. et al., 2021; Liu et al., 2021). In particular, CO_2 injection into deep unminable coal seams offers a promising geological reservoir for simultaneous CO_2 storage and coalbed methane (CBM) recovery (Chiquet et al., 2007; Li et al., 2009; Zepeng et al., 2022). CO_2 exists in the form of $ScCO_2$ when the depth of the coal seams exceeds 800 m, and the pressure and temperature exceed the critical conditions of 7.38 MPa and 31°C (Zhang et al., 2017). Injection of $ScCO_2$ into coal seams, especially those containing water, can cause significant modifications to the pore and fracture structure of the coal due to mineralization reactions between $ScCO_2$-H_2O and minerals. These changes can impact permeability and adsorption capacity in turn (Dawson et al., 2011; Wang Z. et al., 2022). Scholars have conducted extensive research on the interaction of $ScCO_2$ with coal. $ScCO_2$ geochemical reaction experiment on typical high-rank coal of Qinshui Basin was conducted and it is found that $ScCO_2$ dissolved minerals and change the porosity, pore volume and specific surface area of coal (Du et al., 2018). The seepage test before and after CO_2 adsorption were conducted to found that CO_2 adsorption increases the permeability anisotropy of coal due to the high permeability adsorption sensitivity of low permeability cleats and the low permeability adsorption sensitivity of high permeability bedding (Niu et al., 2018). Xiaolei Wang et al. treated coal with subcritical CO_2 and $ScCO_2$, respectively, and found that the solubility of minerals in $ScCO_2$-treated coal is stronger. Furthermore, the total pore volume and BET specific surface area of coal gradually increase with the increase of CO_2 intrusion pressure (Wang X. et al., 2022). Yugang Cheng et al. studied the effects of subcritical and supercritical CO_2 on the pore structure of coal and found that the porosity and pore volume of coal showed an inverted "U" shaped change which first increased and then decreased with the increase of CO_2 pressure (Cheng et al., 2021). M.S.A. Perera et al. conducted adsorption experiments of coal at different CO_2 pressures, indicating that the maximum swelling of coal occurs within 3–4 h after CO_2 injection. And the swelling strain increases while the permeability decreases as CO_2 pressure increases (Perera et al., 2011).

Several studies have highlighted the important role of water in geochemical interactions (Li et al., 2019). Renxia Jiang et al. conducted a $ScCO_2$-H_2O interaction experiment on coal to investigate the effect of $ScCO_2$-H_2O on the primary mineral composition of coal. And the study found that $ScCO_2$ effectively improves the solubility of various elements of coal in water (Jiang et al., 2019). Ruihui Li et al. conducted $ScCO_2$ soaking experiments on bituminous coals with varying moisture contents and investigated the modification of pore characteristics and microcrystalline structure of bituminous coals with the effect of $ScCO_2$ under different moisture conditions (Li R. et al., 2022). Guodong Cui et al. injected water and CO_2 into rock samples, respectively, to investigate the effects of water and CO_2 injection on minerals. The results indicated that mixing the injected water with the original formation water results in significant mineral precipitation, while acidification resulting from the injection of CO_2 leads to the dissolution of some minerals and the precipitation of dolomite, altering the composition of the formation water (Cui et al., 2021). Shasha Gao et al. studied the

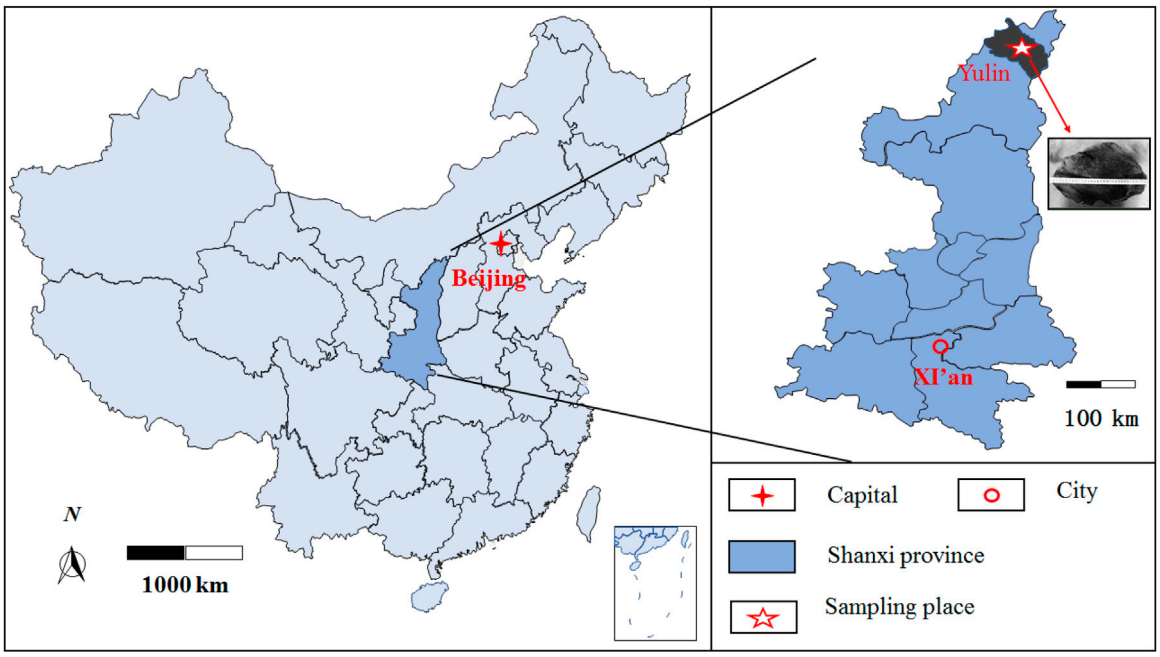

FIGURE 1
Location of coal samples collection.

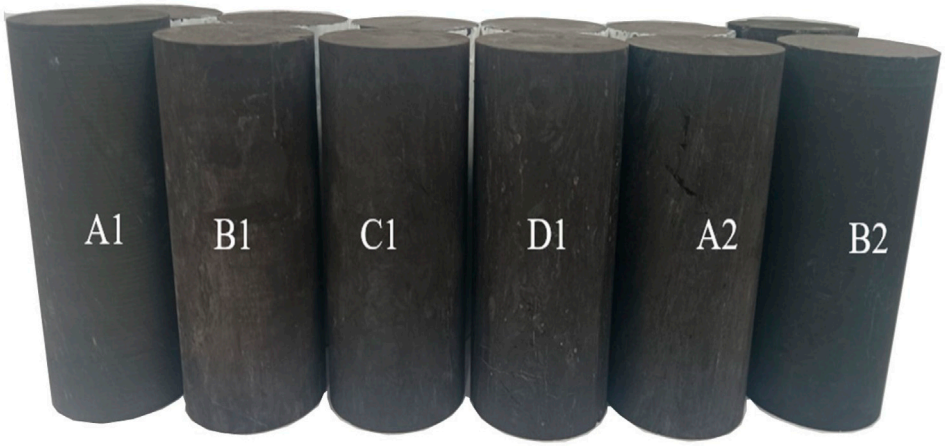

FIGURE 2
The coal samples from Ningtiaota coal mine.

TABLE 1 The groups and treatment conditions of coal samples.

Group	Water-bearing condition	CO_2 pressure/MPa
A	untreated	—
B	dry	8
C	Semi-saturation	8
D	saturation	8

effect of CO_2-H_2O interaction on the pore structure and mineral composition of coal. The results show that the pore structures of coal become more complex due to the geochemical reaction between CO_2-H_2O and carbonate minerals, and the fractures expands and develops after CO_2-H_2O treatment which is positive for permeability (Gao et al., 2022). Yao Song et al. analyzed the influences of the $ScCO_2$–H_2O coupling effect on the microstructures of low-rank coal samples and found that mineral dissolution increases as the CO_2 pressure increases, resulting in an increase in porosity and macropore ratio in the coal samples (Song et al., 2020).

Although the effects of $ScCO_2$ on the pore structure and mineral composition of coal have been extensively studied, most experiments are based on soaking treatment. The hydrological and *in situ* stress conditions of actual coal seams are not be considered (Mirzaeian et al., 2006; Qu et al., 2012; Song et al., 2020; Gao et al., 2022). Therefore, this paper conducted $ScCO_2$ injection experiments on bituminous coal with varying water saturation under *in situ* stress to investigate the influence of $ScCO_2$-H_2O interaction on coal seepage characteristics, pore characteristics, and mineral composition through seepage, low-temperature liquid nitrogen adsorption, and XRD experiments. The findings of this study provide a theoretical guideline for CO_2 geological storage (CGS) and CO_2-enhanced coal bed methane recovery (CO_2-ECBM).

2 Material and methods

2.1 Coal samples

The experiments in this study utilized typical bituminous coal samples from Ningtiaota coal mine, Yulin City, Shanxi Province. The coal was taken from Yan'an Formation. The coal samples were as shown in Figure 1.

Upon on-site collection, the coal was immediately wrapped with plastic and transported to the laboratory. Subsequently, it was cored, polished, and processed into standard cylindrical samples of 50 × 100 dimensions. And the experiments were repeated 2–3 times to ensure the validity of the experimental results. Coal is a natural organic rock with anisotropy. The coal samples used in the tests were all sampled perpendicular to the bedding direction in order to avoid the influence of coal anisotropy on the experimental results (Perera et al., 2011). And the coal samples are depicted in Figure 2.

2.2 Seepage test

The coal samples were divided into different groups based on their water saturation levels achieved through soaking for varying periods of time before the $ScCO_2$ treatment. The specific group numbers and treatment conditions are presented in Table 1.

The coal rock rheology seepage system which was independently developed by the laboratory to simulate the geological environment was used to conduct the seepage tests. And the experimental equipment is illustrated in Figure 3.

Seepage tests were conducted at different axial and confining pressures namely 2.8 MPa and 5.5 MPa as well as 9.8 MPa and 12.5 MPa respectively. The seepage gas pressure was maintained at 3.1 MPa to study changes at different effective stresses. The effective stress acting on the coal sample was calculated using the Terzaghi effective stress formula (Liu Z. et al., 2020):

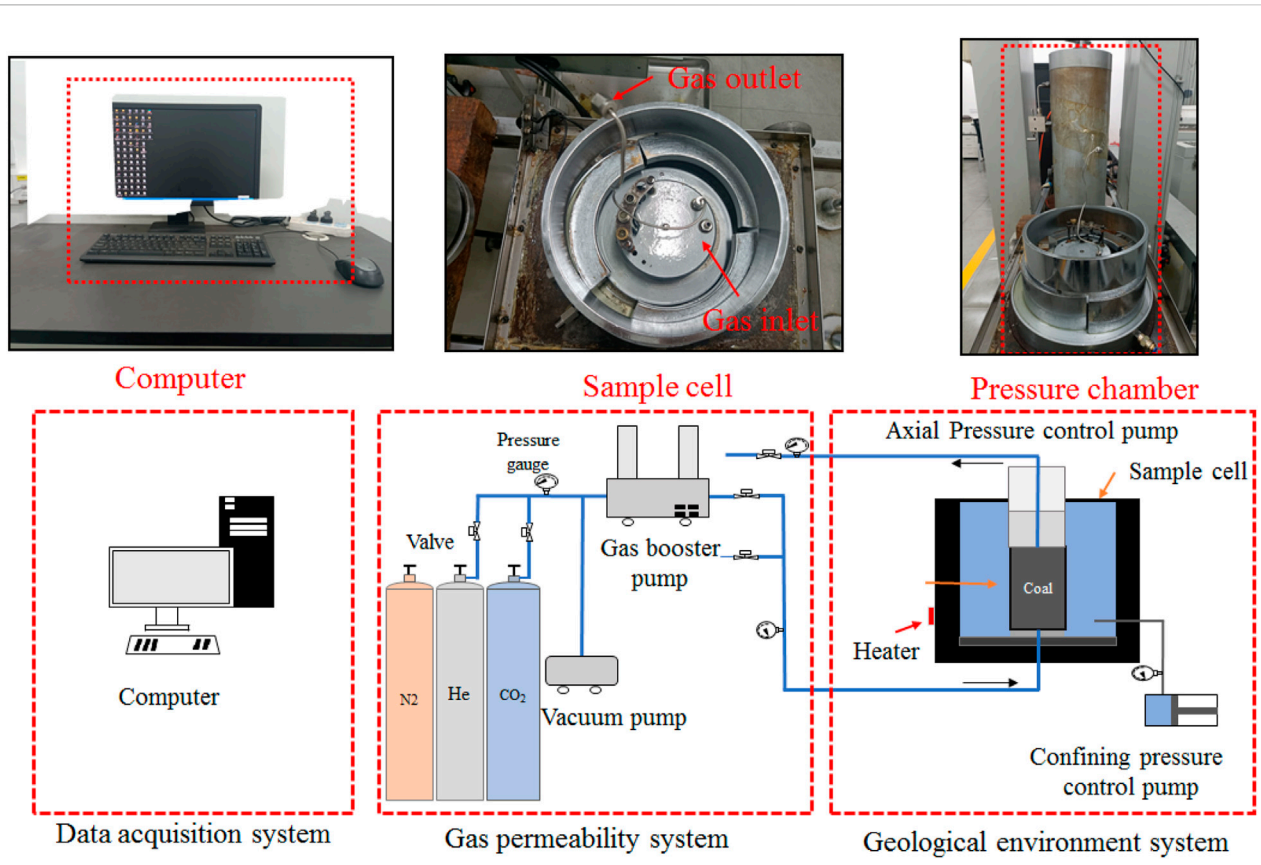

FIGURE 3
The experimental equipment of seepage test.

$$\sigma_e = \frac{1}{3}(\sigma_a + 2\sigma_c) - \frac{1}{2}(P_1 + P_2) \quad (1)$$

Where σ_e is the average effective stress, MPa; σ_a is the axial stress, MPa; σ_c is the confining pressures, MPa; P_1 is the inlet pressure, MPa; P_2 is the outlet pressure, MPa.

The steady-state test method was used in the experiments. For compressible gases, the expansion of fluid can affect the measurement of permeability. Assuming that the permeation of gas through the sample is an isothermal process and that the ideal gas law is applicable. So the gas permeability was calculated according to Darcy's law (Liu X. et al., 2020):

$$k = \frac{2\mu P_a L Q}{A(P_1^2 + P_2^2)} \quad (2)$$

Where k is the permeability, mD; Q is the gas flow rate, cm^3/s; P_a is the atmospheric pressure, 0.1 MPa; A is the cross-sectional area of the sample, cm^2; L is the length of the sample, m; P_1 and P_2 are the inlet and outlet pressures, MPa.

The experimental procedure was conducted as follows: (1) The coal sample was placed in the reaction chamber and the temperature was raised to 35°C. The effective stress was adjusted to 3 MPa and 10 MPa, respectively. Helium (He) was injected to measure the initial permeability of the bituminous coal before $ScCO_2$ treatment. (2) The He injection was stopped, and the axial and radial stress were adjusted to 10 MPa to simulate geological conditions at a depth of 1,000 m underground (Du et al., 2020). Then, $ScCO_2$ of 8 MPa was injected after discharging the residual gas. Previous studies have pointed out that the maximum expansion strain occurs within 3–4 h after CO_2 injection, so an 8-hour period is sufficient to investigate the effect of $ScCO_2$-H_2O on coal. And the coal samples were left to fully absorb and react for 8 h (Cheng et al., 2021). (3) After complete CO_2 adsorption and desorption of the coal samples, step (1) was repeated to measure the permeability of the coal sample after $ScCO_2$ treatment.

2.3 Low temperature liquid nitrogen adsorption test

The low temperature liquid nitrogen adsorption tests were conducted by using a fully automated multistation specific surface area and pore size analyzer, Quadrasorb 2 MP, manufactured by Conta Instruments, USA. Prior to the experiments, the coal samples were processed into 60–80 mesh powder and then pretreated by drying and degassing at 110°C for 24 h. The tests were used to measure the specific surface area, pore size distribution, and pore volume of the coal samples.

2.4 XRD test

The mineral components of the coal samples were analyzed by using a high efficiency conventional powder X-ray diffractometer

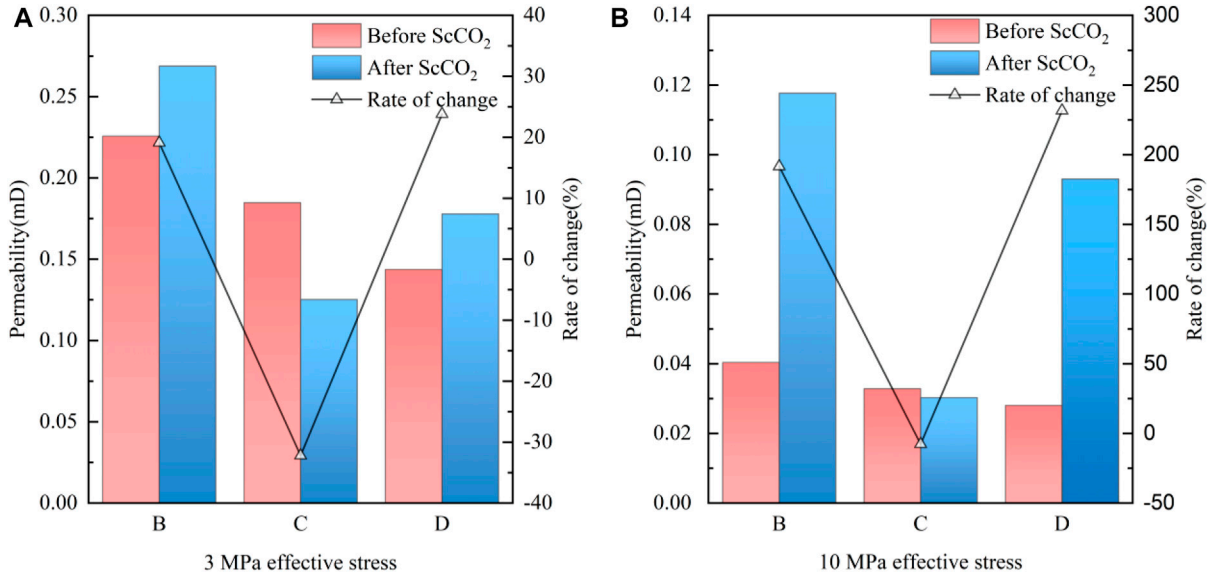

FIGURE 4
Permeability of the coal samples before and after $ScCO_2$ treatment at different effective stresses. **(A)** 3 MPa effecitve stress, **(B)** 10 MPa effective stress.

from Spectris, the Netherlands. The coal samples were ground into a powder of 200 mesh size and were pretreated prior to the experiments. The crystallographic information of the coal samples was obtained by scanning angles ranging from 5°–80° with a scanning time of 20 min.

3 Results and Discusssion

3.1 Permeability characteristics

He seepage tests were performed on bituminous coal samples with varying water saturation levels before and after treatment to examine the effects of $ScCO_2$-H_2O on permeability characteristics. Figure 4 presents the measured permeability values.

Figure 4 indicates that the permeability of bituminous coal is primarily influenced by the moisture content of the coal samples prior to $ScCO_2$ treatments (Zhang X. et al., 2019). Specifically, the permeability of coal samples declines from 0.226 mD to 0.144 mD with the increase of water saturation at 3 MPa effective stress. Similarly, the permeability of coal samples drops from 0.040 mD to 0.028 mD as water saturation increases at 10 MPa effective stress, which aligns with earlier research findings (Pan et al., 2010). The decline can be attributed to the combination of seepage channels such as the pores blockage by water and the squeezing effect caused by internal water absorption expansion (Teng et al., 2017; Talapatra et al., 2020). Moreover, the permeability of coal samples decreases due to compression of the seepage channels caused by increased stress as effective stress increases, which was the result of the continuous closure of pores and fractures as the effective stress increases (Niu et al., 2019).

In order to describe the changes of coal samples' permeability before and after $ScCO_2$ treatment better, the permeability change index k_c of coal samples is defined as follows:

$$k_c = \frac{k_1 - k_0}{k_0} \times 100\% \quad (3)$$

Where, k_0 is the permeability before $ScCO_2$ treatment, mD; k_1 is the permeability after $ScCO_2$ treatment, mD; k_c is the permeability change index, %.

Upon comparing the permeability of coal samples before and after $ScCO_2$ treatment, it is evident that the permeability of samples B and D increased after CO_2 treatment. The permeability of sample B increased from 0.226 mD to 0.269 mD at 3 MPa effective stress with the growth rate of 19.09%. Similarly, the permeability of sample D increased from 0.144 mD to 0.178 mD at 3 MPa effective stress with a growth rate of 23.81%. The physical-chemical reactions of $ScCO_2$ on the minerals of coal samples such as dissolution and extraction resulted in the widening of pores and fractures and improved pore connectivity, leading to an increase of permeability (Zhang G. et al., 2019). Moreover, the permeability of sample B increased from 0.040 mD to 0.118 mD at 10 MPa effective stress with a growth rate of 191.53%, and sample D's permeability increased from 0.028 mD to 0.093 mD with a growth rate of 231.71%. The k_c of sample D is much higher than that of sample B. Because the increase in moisture in the coal samples promotes the dissolution of internal minerals, which broadens and connects the pores better. Moreover, the k_c of coal samples at 10 MPa effective stress was found to be much higher than the k_c at 3 MPa effective stress. Because the cracks in the coal samples are largely closed as the effective stress increases. Therefore, the permeability of coal samples is controlled by pores at high effective stress, while it is controlled by fractures at low effective stress. The contact area between $ScCO_2$-H_2O and pore surface is larger, the reaction is more sufficient, and the pore connectivity is better. Therefore, the growth of permeability is more obvious at high effective stress.

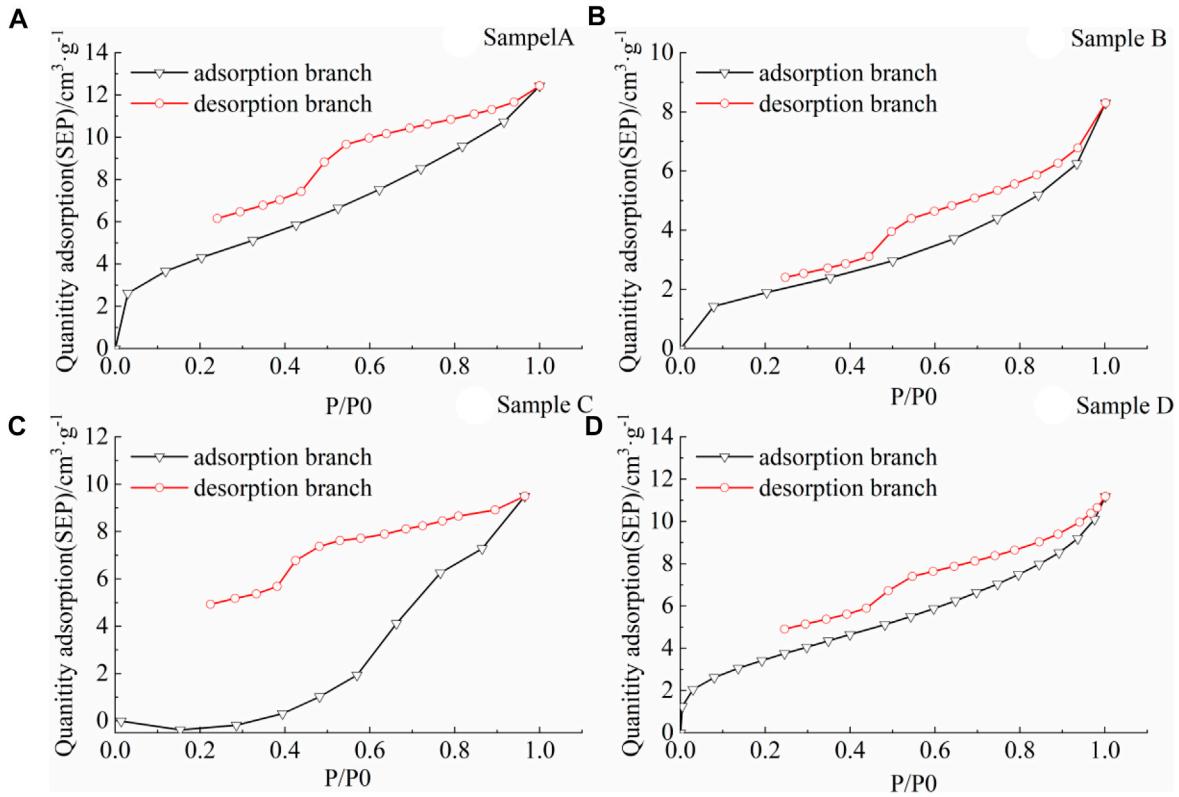

FIGURE 5
Low temperature liquid nitrogen adsorption-desorption curve. **(A)** sample A, **(B)** sample B, **(C)** sample C, **(D)** sample D.

Additionally, Figure 4 shows that the permeability of sample C decreases after $ScCO_2$ treatment. There are two possible reasons for the phenomenon. Firstly, the *in situ* stress conditions may have caused the collapse of the pores in the coal samples, leading to the blockage of seepage channels despite the modification of pore fissures by $ScCO_2$. Secondly, $ScCO_2$ treatment may have caused the generation of new mineral precipitations in sample C, which could have blocked the pore channels and had a negative impact on the permeability.

3.2 Pore characteristics

Coal is a naturally occurring organic rock with a dual pore structure that is influenced by various factors such as the freeze-thaw effect, effective stress and the action of $ScCO_2$ (Huang et al., 2017; Li et al., 2020; Chen et al., 2022). The pore structure is considered to be the most significant factor affecting the efficiency of ECBM and the stability of CGS (Wang et al., 2015; Zhang et al., 2020). The strong interaction of $ScCO_2$-H_2O and coal results in significant changes in the pore structure (Pan et al., 2018). The low temperature liquid nitrogen adsorption tests were conducted on coal samples before and after $ScCO_2$ treatment to investigate the effect of $ScCO_2$ on the pore characteristics of water-bearing coal samples. The adsorption and desorption capacity at different relative pressures were measured, and important parameters such as adsorption-desorption isotherms, pore size distribution, pore volume, specific surface area, and average pore size were calculated (Yi et al., 2012; Ni et al., 2020; Liu et al., 2022).

Experiments were conducted on both the original coal (sample A) and the $ScCO_2$-treated coal (samples B, C and D), and the resulting adsorption-desorption curves are displayed in Figure 5. The curves demonstrate varying trends, which can be classified into two types based on their morphological characteristics as defined in this paper.

Type A is characterized by a sharp decrease in the desorption branch at the relative pressure of 0.9–1.0, followed by a slow decrease as the relative pressure decreases. Then there is a certain decreasing inflection point at the relative pressure of about 0.5. When the relative pressure is below 0.1, the adsorption and desorption branches are not closed, and the distance between them is relatively small (Figures 5A, B, D). This type is caused by the existence of permeable pores with open ends and ink bottle type pores in the coal samples.

Similar to Type A, type B is characterized by a sharp decrease in the desorption branch at the relative pressure of 0.9–1.0, followed by a slow decrease as the relative pressure decreases. Then there is a certain inflection point at the relative pressure of about 0.5. When the relative pressure is below 0.1, the adsorption and desorption branches are not completely closed, and the distance between them is relatively large (Figure 5C). This type is caused by the development of pore narrow crevice pores, ink bottle pores, and permeable pores with open ends of the coal samples.

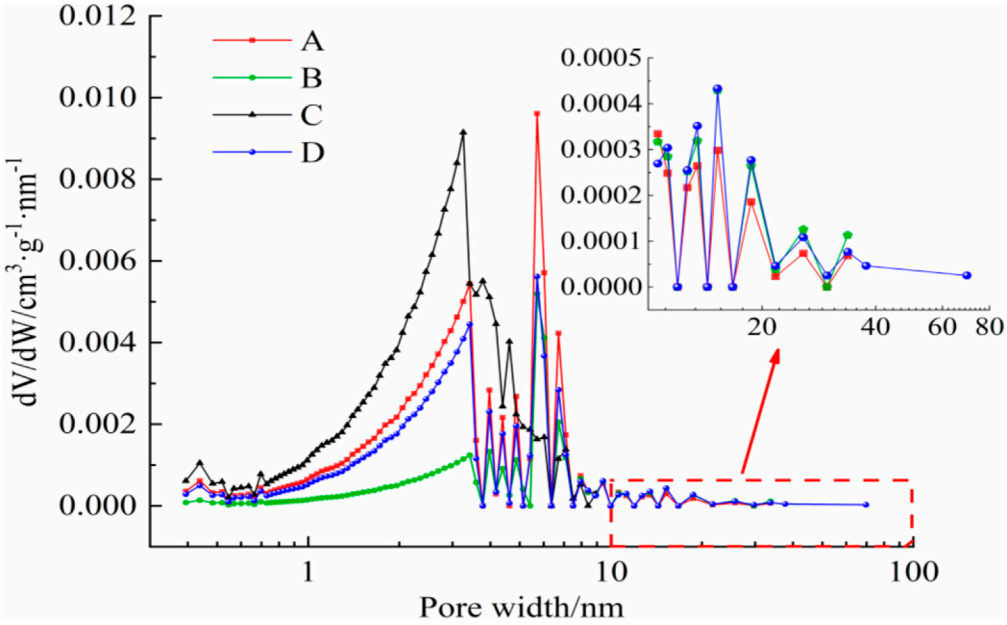

FIGURE 6
Pore size distribution characteristics of the coal samples.

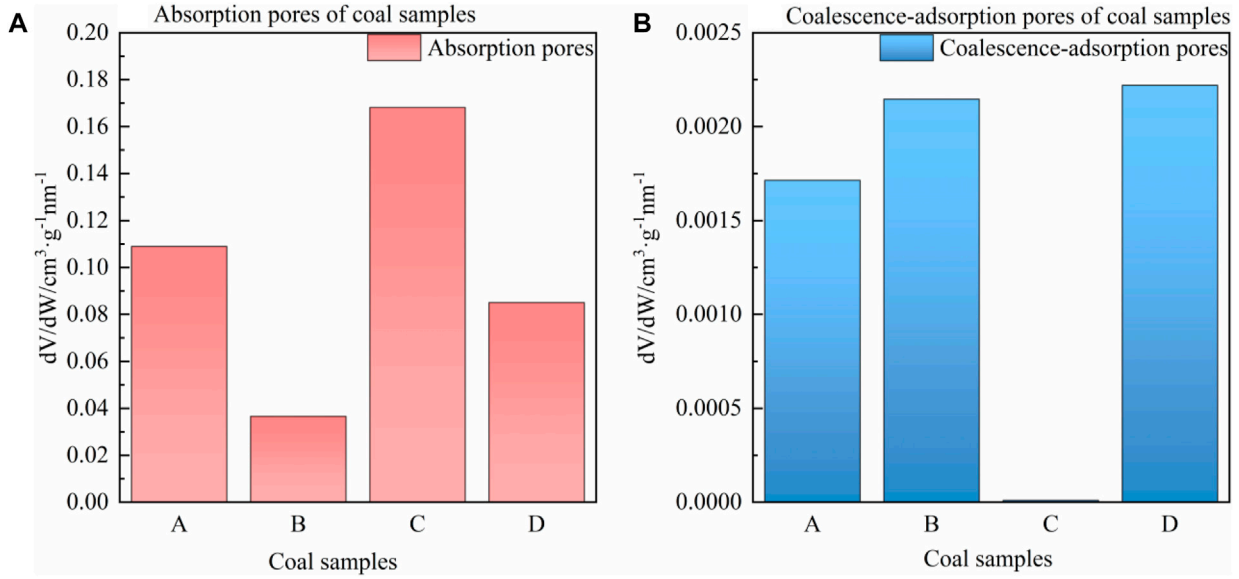

FIGURE 7
Adsorption pore volume of coal samples. **(A)** Adsorption pores, **(B)** Coalescence-adsorption pores.

Based on Kelvin's capillary coalescence theory, we used the BJH pore size analysis model to analyze the pores in the paper, which is widely accepted (Hu et al., 2021). The pore size distribution of the coal samples was plotted with BJH pore size (W) as the horizontal coordinate and the differential of pore volume to pore size (dV/dW) as the vertical coordinate, as shown in Figure 6.

The pore size distribution curves of the four coal samples in Figure 6 show similar trends that most pores falling within the 1–10 nm size range, and two main peaks observed between 2–5 nm and 5–8 nm. Additionally, there are several small peaks in the 10 nm range for three of the coal samples. As can be seen from Figure 6, the pore sizes of samples B and D tend to increase, while the pore sizes of

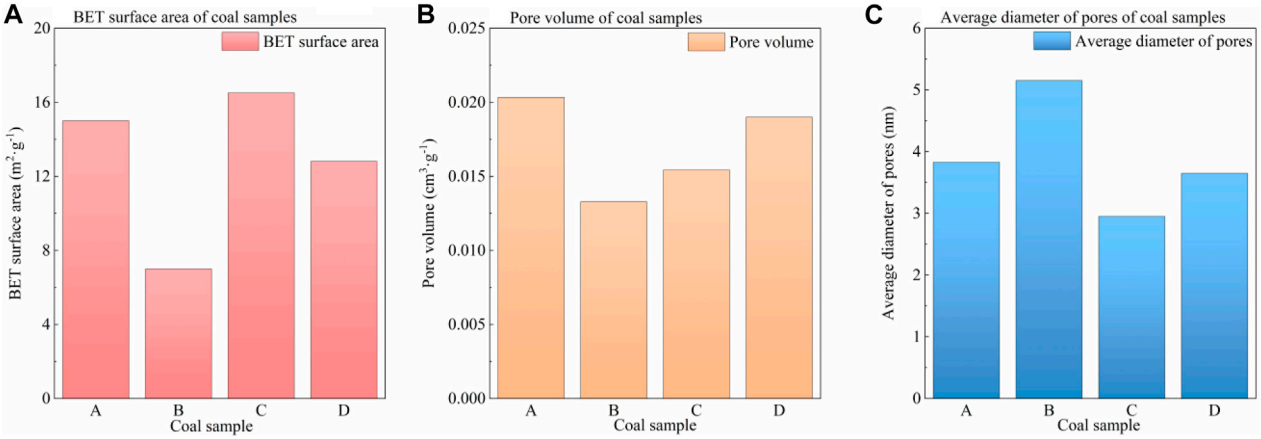

FIGURE 8
Pore parameters of coal samples. **(A)** BET surface area, **(B)** Pore volume, **(C)** Average diameter of pores.

sample C tend to decrease. Coal pore sizes can generally be categorized into adsorption pores (<100 nm) and seepage pores (>100 nm) (Mou et al., 2021). And the adsorption pores can be divided into coagulation-adsorption pores (10–100 nm) and absorption pores (<10 nm) further (Ni et al., 2020). The results in Figure 6 indicate that the pore size distribution of coal samples changed significantly after $ScCO_2$ treatment. Consequently, the volumes of adsorption pores and coagulation-adsorption pores for each of the four coal samples were calculated and are shown in Figure 7.

As depicted in Figure 7, the pore volumes of the four coal samples display distinct changes. Samples B and D show a decrease in the adsorption pore volumes, while sample C exhibits an increase. Conversely, the volumes of the coalescence-adsorption pore of samples B and D increase, while sample C shows a decrease. These findings indicate that the pores of coal samples undergo transformations after $ScCO_2$ treatment, where the pore size of samples B and D increases while the pore size of sample C decreases. Based on the changes in pore size, the samples can be categorized as either pore broadening type (samples B, D) or pore shrinkage type (sample C). The trend in pore changes in coal samples is consistent with the permeability changes discussed earlier. The BJH pore size analysis model was employed to determine the average pore size, pore volume, and specific surface area of the four coal samples. The specific parameters are presented in Figure 8.

Figure 8A shows that the specific surface area of samples B and D decreased after $ScCO_2$ treatment compared to raw coal (sample A) before $ScCO_2$ treatment. This is caused by the conversion of adsorption pores into seepage pores in coal samples, which is not conducive to gas adsorption. In contrast, the specific surface area of sample C increased after $ScCO_2$ treatment, providing more space for CO_2 adsorption and improving the stability of CO_2 sequestration.

It is evident that the pore volumes of samples B, C, and D decreased to varying degrees in Figure 8B. The decrease in pore volumes of the three coal samples is caused by axial and radial stress compression during $ScCO_2$ treatment. Then the transformation effect of $ScCO_2$ on coal is enhanced as the water content increases, and the pore volume of coal samples is restored to a certain extent. Therefore, the pore volume of coal samples continuously increases as the water content increases.

Figure 8C illustrates that the average pore size of sample B increases, while the average pore size of samples C and D decreases. This trend is opposite to that of the specific surface area due to the fact that the small pores provide more specific surface area than large pores.

The results above indicate that $ScCO_2$ promotes the development of seepage pores in dry and water saturated coal samples, leading to an increase in permeability and enhancement of CBM extraction efficiency. Furthermore, $ScCO_2$ causes the transformation of macropores into micropores and small pores of the half-saturated coal samples, providing more space for CO_2 adsorption and improving the capacity of CO_2 sequestration.

3.3 Mineral composition

XRD tests were performed on the four coal samples. The resulting data were analyzed by Jade 6 software to determine the mineral composition of the different water-saturated coal samples, which is shown in Figure 9. The analysis reveals that the minerals present in the raw coal samples include 25.1% calcite ($CaCO_3$), 20.0% dolomite ($CaMg(CO_3)_2$), 15.1% quartz (SiO_2), 2.3% pyrite (FeS_2), and 37.5% clay minerals, with illite ($K_3Fe_4Si1_4Al_7O_{40}(OH)_8$) and kaolinite ($Al_2Si_2O_5(OH)_4$) accounting for 11.2% and 26.3% of the clay minerals, respectively.

As shown in Figure 9, the $ScCO_2$ treatment resulted in a decrease in the content of carbonate minerals and an increase in the content of clay minerals in samples B, C, and D. This can be attributed to the strong dissolution reaction of carbonate minerals which are more sensitive to acidic environments (Zhang K. et al., 2019; Fatah et al., 2021; Ozotta et al., 2021). Although clay minerals can also be dissolved, the reaction rate is relatively slow, leading to an increase in their content. Specifically, the dolomite in sample B was violently dissolved, while calcite was slowly dissolved, resulting in a relatively higher content of the remaining minerals. Similarly,

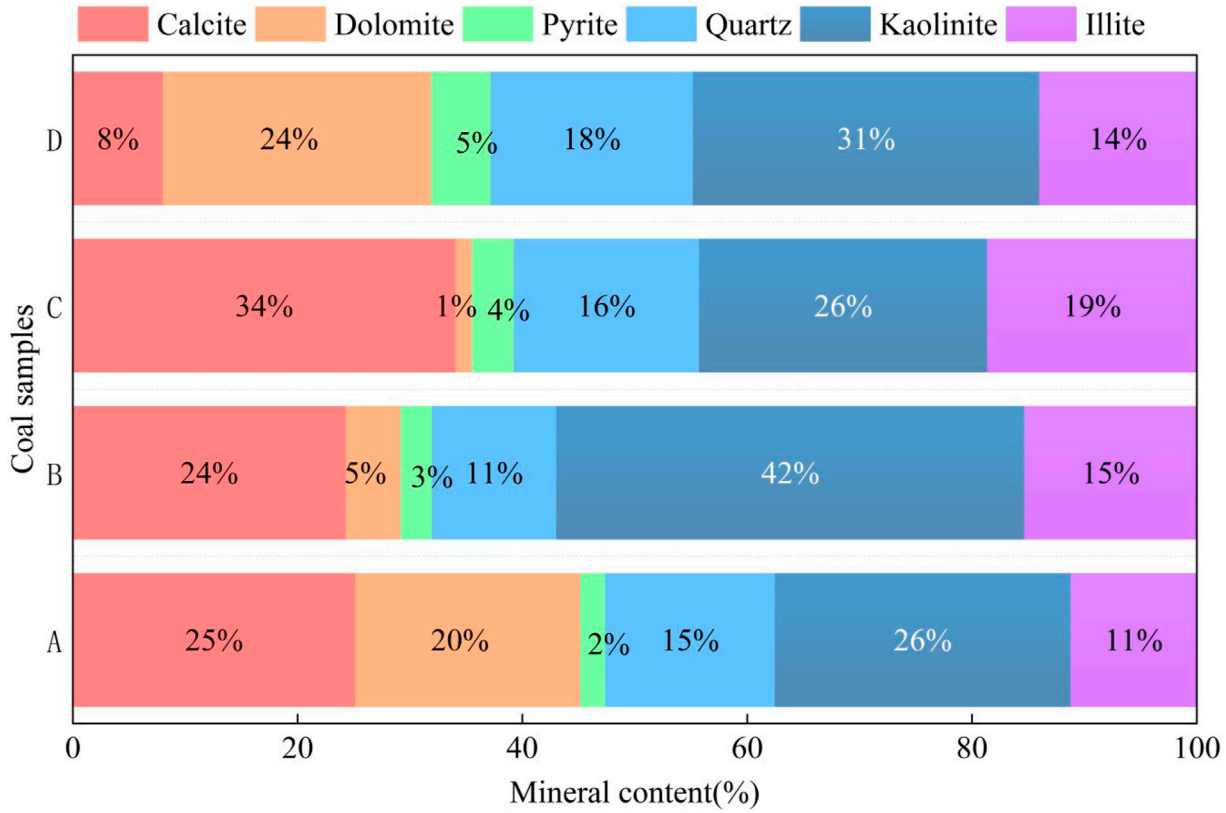

FIGURE 9
Mineral content changes.

the violent dissolution of calcite led to a relatively higher content of other minerals in sample D. The reaction above promoted the expansion of pores in samples B and D and improved the connectivity of pores. Therefore, their adsorption pores decrease and permeability increases.

Notably, the content of dolomite in sample C decreased significantly, while the content of calcite increased. This can be explained by the fact that the water in sample C reduced the pH value of the solution compared to sample D, intensifying the dissolution of dolomite. However, the large amount of Ca^{2+} and Mg^{2+} generated by the dolomite reaction could not be completely dissolved by the water in coal sample C. Moreover, the solubility of Ca^{2+} is lower than that of Mg^{2+}, causing Ca^{2+} to combine with CO_3^{2-} to precipitate as new calcite and increase the relative content of calcite. Moreover, a large amount of newly formed calcite precipitates in key seepage channels such as pore throats, dividing the original pores, resulting in an increase in BET specific surface area and a decrease in permeability.

3.4 Reaction mechanism

The combination of $ScCO_2$ and water generates H_2CO_3, which has strong extraction and corrosion effects on coal. Consequently, the microstructure of coal samples with different water saturation changes drastically after $ScCO_2$ treatment, leading to changes of permeability. The transformation mechanism is illustrated in Figure 10.

There is a series of geochemical reactions minerals in coal after $ScCO_2$ injection, and the specific reactions are as follows (Wang Z. et al., 2021; Ozotta et al., 2021):

$$CO_2 + H_2O \rightarrow H^+ + HCO_3^- \rightarrow H^+ + CO_3^{2-} \quad (4)$$

$$CaCO_3 + 2H^+ \rightarrow Ca^{2+} + H_2O + CO_2 \quad (5)$$

$$CaMg(CO_3)_2 + 4H^+ \rightarrow Ca^{2+} + Mg^{2+} + 2H_2O + 2CO_2 \quad (6)$$

$$FeS_2 + 2H^+ \rightarrow Fe^{2+} + H_2S + S \quad (7)$$

$$Al_2Si_2O_5(OH)_4 + 6H^+ \rightarrow 2Al^{3+} + 2SiO_2 + 5H_2O \quad (8)$$

$$K_3Fe_4Si_{14}Al_7O_{40}(OH)_8 + 88H^+ \rightarrow 7Al^{3+} + 3K^+ + 4Fe^{2+} + 14Si^{4+} + 48H_2O \quad (9)$$

Dolomite in the coal samples undergoes significant dissolution after $ScCO_2$ treatment, while the dissolution rate of clay minerals is relatively slow, resulting in an increased content of clay minerals. The content of quartz increases as the water saturation increases, although it does not undergo any significant reaction. This can be attributed to two reasons: (1) the dissolution of clay minerals produces new quartz minerals; (2) the violent dissolution of carbonate minerals leads to the relative increase in the content of quartz due to a decrease in the content of carbonate minerals.

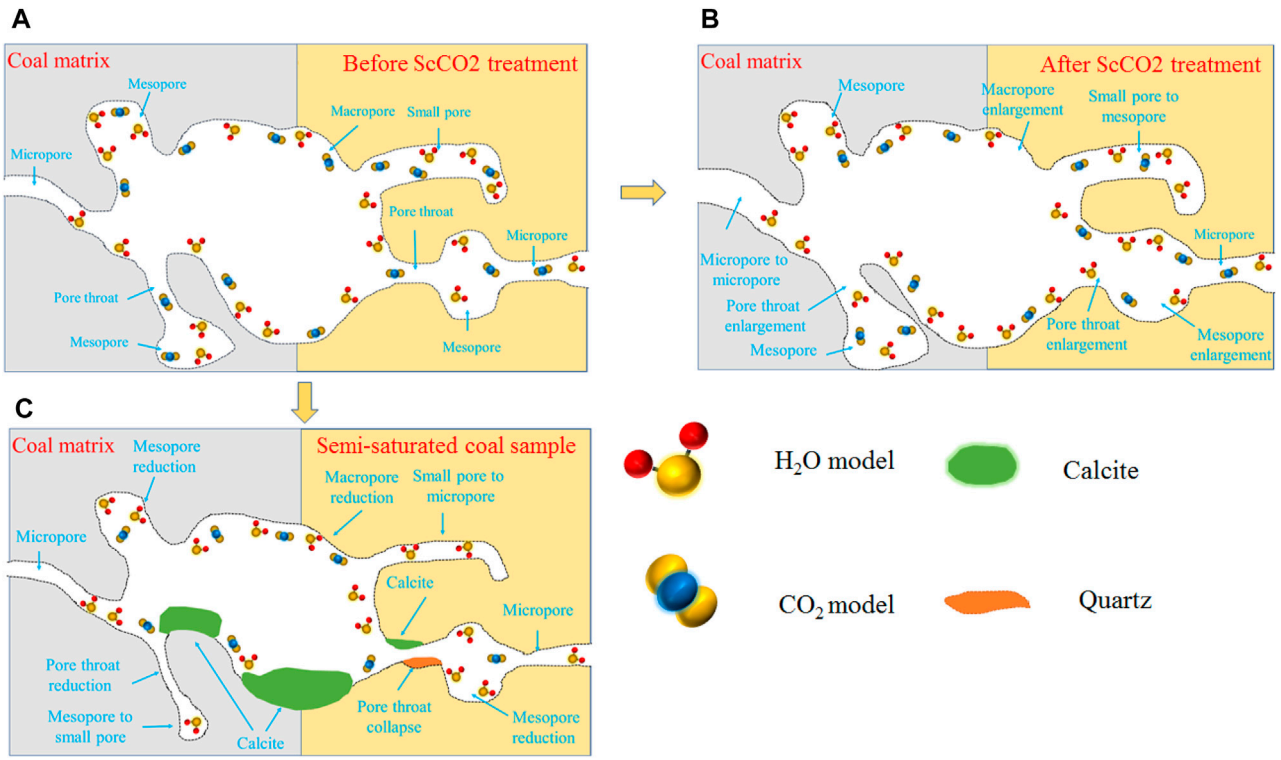

FIGURE 10
Reaction mechanism. **(A)** Before $ScCO_2$ treatment, **(B)** After $ScCO_2$ treatment, **(C)** Semi-saturated coal sample.

In Figure 10B, it can be observed that the injection of $ScCO_2$ results in significant dissolution of carbonate minerals in samples B and D. This dissolution widens the original pores and fractures, transforms the micropores into macropores, and improves the connectivity of seepage channels, thus enhancing the permeability of the coal samples. The formation of H_2CO_3 due to the CO_2-H_2O reaction in sample D leads to a lower pH and faster dissolution rate of carbonate minerals. Additionally, the presence of sufficient water increases the solubility of Ca^{2+} and Mg^{2+} which promotes the reaction progress and increases the connectivity of seepage pores further (Jiang et al., 2019). Therefore, the permeability growth of sample D is higher after $ScCO_2$ treatment comparing to sample B. However, this reaction also results in a reduction of initial adsorption pores and BET specific surface area, which is negative for CO_2 adsorption and stable storage.

In Figure 10C, it is shown that the dissolution of dolomite in sample C results in a substantial increase in Ca^{2+} and Mg^{2+}. However, the water in the sample C is unable to dissolve these ions completely comparing to sample D. As a result, the Ca^{2+} combines with CO_3^{2-} in the solution, leading to the precipitation of calcite. The newly formed calcite aggregates in the original seepage channels and pore throats, obstructing the seepage channels and reducing the size of the original macropores. This leads to a decrease in the pore size and an increase in the specific BET surface area of the coal samples. Consequently, the permeability of sample C decreases. However, the increased BET specific surface area provides more sites for CO_2 adsorption.

The fractures in coal samples are closed at high stress conditions, and the permeability is controlled by the seepage pores. However, the contact area between the $ScCO_2$ and pores surface is greater comparing to fractures, and the reaction is more efficient, resulting in better transformation effects. Therefore, the seepage growth of coal samples at high stress conditions is higher.

4 Conclusion

The $ScCO_2$-H_2O reaction experiments on coal samples with varying water saturation levels at *in situ* stress were conducted. Then the seepage tests, low temperature liquid nitrogen adsorption tests, and XRD tests was conducted to analyze the changes of the samples before and after treatment. The key findings are summarized below:

(1) $ScCO_2$ treatment significantly increases the permeability of both dry and water saturated coal samples at *in situ* stress conditions, which is more effective for water saturated coal samples. The growth rates of permeability as the effective stress increases due to the improved pore transformation. However, the permeability of semi-saturated coal samples decreases after $ScCO_2$ treatment due to the effects of stress compression and seepage channel blockage caused by new mineral precipitation.
(2) The low temperature liquid nitrogen adsorption tests revealed that $ScCO_2$ treatment effectively increased the pore size of dry and water saturated coal samples. And the pore volume of coal samples increases as the moisture content increases. However,

$ScCO_2$ treatment significantly increased the size of adsorption pores in semi-saturated coal samples, which provided more space for CO_2 adsorption.

(3) XRD analysis showed that $ScCO_2$ treatment makes the carbonate mineral content decrease and silicate minerals content increase in coal samples, which facilitated pore connectivity. Although the dissolution of dolomite increased the pore size of semi-saturated coal samples, the newly formed calcite and quartz clogged the pore throats and divided the pores, leading to a reduction in seepage pores.

(4) The experimental and analytical results show that the reaction mechanism of coal samples with different moisture content after $ScCO_2$ injection is different. $ScCO_2$ effectively improves the pore connectivity of dry and water saturated coal samples. This effect is even greater for saturated coal samples. Although the pores of semi saturated coal samples have been expanded after $ScCO_2$ treatment, the newly formed minerals such as quartz and calcite have a negative impact on pore connectivity and permeability.

The study compared the changes of mineral composition, pore structure, and permeability of coal samples with different water saturations before and after $ScCO_2$ treatment, and the change mechanism of bituminous coal with different water saturations was analyzed, which is significant for CGS and ECBM. However, the explanation for the change of semi-saturated bituminous coal after $ScCO_2$ treatment is still unclear. Therefore, it is necessary to further analyze the change rules and mechanisms of bituminous coal with different moisture content under the action of $ScCO_2$ in detail.

Data availability statement

The original contributions presented in the study are included in the article/supplementary material, further inquiries can be directed to the corresponding authors.

Author contributions

CL, JZ, and SH conceived and designed the experiments; CL performed the experiments; CL analyzed the data; CL and JZ contributed materials and analysis tools; CL and JZ wrote the paper. SH reviewed and edited.

Funding

The authors acknowledge fundings by National Natural Science Foundation of China (No. 42202155), China Postdoctoral Science Foundation (No. 2021MD703807), Heilongjiang Provincial Postdoctoral Science Foundation (No. LBH-Z20121).

Acknowledgments

We thank Chongqing University and Northeast Petroleum University for the financial support to this study.

Conflict of interest

The authors declare that the research was conducted in the absence of any commercial or financial relationships that could be construed as a potential conflict of interest.

Publisher's note

References

Chen, K., Liu, X., Nie, B., Zhang, C., Song, D., Wang, L., et al. (2022). Mineral dissolution and pore alteration of coal induced by interactions with supercritical CO_2. *Energy* 248, 123627. doi:10.1016/j.energy.2022.123627

Cheng, Y., Zhang, X., Lu, Z., Pan, Z. j., Zeng, M., Du, X., et al. (2021). The effect of subcritical and supercritical CO2 on the pore structure of bituminous coals. *J. Nat. Gas. Sci. Eng.* 94, 104132. doi:10.1016/j.jngse.2021.104132

Chiquet, P., Daridon, J.-L., Broseta, D., and Thibeau, S. (2007). CO_2/water interfacial tensions under pressure and temperature conditions of CO_2 geological storage. *Energy Convers. manage.* 48 (3), 736–744. doi:10.1016/j.enconman.2006.09.011

Cui, G., Yang, L., Fang, J., Qiu, Z., Wang, Y., and Ren, S. (2021). Geochemical reactions and their influence on petrophysical properties of ultra-low permeability oil reservoirs during water and CO_2 flooding. *J. Pet. Sci. Eng.* 203, 108672. doi:10.1016/j.petrol.2021.108672

Dawson, G. K. W., Golding, S. D., Massarotto, P., and Esterle, J. S. (2011). Experimental supercritical CO_2 and water interactions with coal under simulated *in situ* conditions. *Energy Procedia* 4, 3139–3146. doi:10.1016/j.egypro.2011.02.228

Du, Y., Fu, C., Pan, Z., Sang, S., Wang, W., Liu, S., et al. (2020). Geochemistry effects of supercritical CO_2 and H_2O on the mesopore and macropore structures of high-rank coal from the Qinshui Basin, China. *Int. J. Coal Geol.* 223, 103467. doi:10.1016/j.coal.2020.103467

Du, Y., Sang, S., Wang, W., Liu, S., Wang, T., and Fang, H. (2018). Experimental study of the reactions of supercritical CO_2 and minerals in high-rank coal under formation conditions. *Energy Fuel* 32 (2), 1115–1125. doi:10.1021/acs.energyfuels.7b02650

Fatah, A., Mahmud, H. B., Bennour, Z., Hossain, M., and Gholami, R. (2021). Effect of supercritical CO_2 treatment on physical properties and functional groups of shales. *Fuel* 303, 121310. doi:10.1016/j.fuel.2021.121310

Gao, S., Jia, L., Zhou, Q., Cheng, H., and Wang, Y. (2022). Microscopic pore structure changes in coal induced by a CO_2-H_2O reaction system. *J. Pet. Sci. Eng.* 208, 109361. doi:10.1016/j.petrol.2021.109361

Hu, Z., Li, C., and Zhang, D. (2021). Interactions of dynamic supercritical CO_2 fluid with different rank moisture-equilibrated coals: Implications for CO_2 sequestration in coal seams. *Chin. J. Chem. Eng.* 35, 288–301. doi:10.1016/j.cjche.2020.10.020

Huang, S., Liu, D., Yao, Y., Gan, Q., Cai, Y., and Xu, L. (2017). Natural fractures initiation and fracture type prediction in coal reservoir under different *in-situ* stresses during hydraulic fracturing. *J. Nat. Gas. Sci. Eng.* 43, 69–80. doi:10.1016/j.jngse.2017.03.022

Jiang, R., and Yu, H. (2019). Interaction between sequestered supercritical CO_2 and minerals in deep coal seams. *Int. J. Coal Geol.* 202, 1–13. doi:10.1016/j.coal.2018.12.001

Li, R., Ge, Z., Wang, Z., Zhou, Z., Zhou, J., and Li, C. (2022b). Effect of supercritical carbon dioxide ($ScCO_2$) on the microstructure of bituminous coal with different moisture contents in the process of $ScCO_2$ enhanced coalbed methane and CO_2 geological sequestration. *Energy Fuel.* 36 (7), 3680–3694. doi:10.1021/acs.energyfuels.1c04027

Li, X., Wei, N., Liu, Y., Fang, Z., Dahowski, R. T., and Davidson, C. L. (2009). CO_2 point emission and geological storage capacity in China. *Energy Procedia* 1 (1), 2793–2800. doi:10.1016/j.egypro.2009.02.051

Li, X., Yu, H., Lebedev, M., Lu, M., Yuan, Y., Yang, Z., et al. (2022a). The influence of CO2 saturated brine on microstructure of coal: Implications for carbon geo-sequestration. *Front. Energy Res.* 10. doi:10.3389/fenrg.2022.802883

Li, Y., Tang, S., Zhang, S., Xi, Z., and Wang, P. (2019). Biogeochemistry and water–rock interactions of coalbed methane Co-produced water in the shizhuangnan block of the southern Qinshui Basin, China. *China.* ***Water*** 12 (1), 130. doi:10.3390/w12010130

Li, Z., Yang, G., and Liu, H. (2020). The influence of regional freeze–thaw cycles on loess landslides: Analysis of strength deterioration of loess with changes in pore structure. *Water* 12 (11), 3047. doi:10.3390/w12113047

Liu, J., Xie, L., He, B., Gan, Q., and Zhao, P. (2021). Influence of anisotropic and heterogeneous permeability coupled with *in-situ* stress on CO2 sequestration with simultaneous enhanced gas recovery in shale: Quantitative modeling and case study. *Int. J. Greenh. Gas Control* 104, 103208. doi:10.1016/j.ijggc.2020.103208

Liu, J., Xie, L., Yao, Y., Gan, Q., Zhao, P., and Du, L. (2019). Preliminary study of influence factors and estimation model of the enhanced gas recovery stimulated by carbon dioxide utilization in shale. *ACS Sustain. Chem. Eng.* 7 (24), 20114–20125. doi:10.1021/acssuschemeng.9b06005

Liu, S., Yang, K., Sun, H., Wang, D., Zhang, D., Li, X., et al. (2022). Adsorption and deformation characteristics of coal under liquid nitrogen cold soaking. *Fuel* 316, 123026. doi:10.1016/j.fuel.2021.123026

Liu, X., Yu, J., Wu, D., and Xiao, X. (2020b). Permeability characteristics of coal after supercritical CO_2 adsorption at different temperatures. *Geofluids* 2020, 1–8. doi:10.1155/2020/8836349

Liu, Z., Liu, D., Cai, Y., and Pan, Z. (2020a). Experimental study of the effective stress coefficient for coal anisotropic permeability. *Energy Fuel.* 34 (5), 5856–5867. doi:10.1021/acs.energyfuels.0c00907

Mirzaeian, M., and Hall, P. J. (2006). The interactions of coal with CO_2 and its effects on coal structure. *Energy Fuel.* 20 (5), 2022–2027. doi:10.1021/ef060040+

Mou, P., Pan, J., Niu, Q., Wang, Z., Li, Y., and Song, D. (2021). Coal pores: Methods, types, and characteristics. *Energy Fuel.* 35 (9), 7467–7484. doi:10.1021/acs.energyfuels.1c00344

Ni, G., Li, S., Rahman, S., Xun, M., Wang, H., Xu, Y., et al. (2020). Effect of nitric acid on the pore structure and fractal characteristics of coal based on the low-temperature nitrogen adsorption method. *Powder Technol.* 367, 506–516. doi:10.1016/j.powtec.2020.04.011

Niu, Q., Cao, L., Sang, S., Zhou, X., and Liu, S. (2019). Experimental study of permeability changes and its influencing factors with CO_2 injection in coal. *J. Nat. Gas. Sci. Eng.* 61, 215–225. doi:10.1016/j.jngse.2018.09.024

Niu, Q., Cao, L., Sang, S., Zhou, X., and Wang, Z. (2018). Anisotropic adsorption swelling and permeability characteristics with injecting CO_2 in coal. *Energy Fuel.* 32 (2), 1979–1991. doi:10.1021/acs.energyfuels.7b03087

Ozotta, O., Ostadhassan, M., Liu, K., Liu, B., Kolawole, O., and Hadavimoghaddam, F. (2021). Reassessment of CO_2 sequestration in tight reservoirs and associated formations. *J. Pet. Sci. Eng.* 206, 109071. doi:10.1016/j.petrol.2021.109071

Pan, Y., Hui, D., Luo, P., Zhang, Y., Sun, L., and Wang, K. (2018). Experimental investigation of the geochemical interactions between supercritical CO_2 and shale: Implications for CO_2 storage in gas-bearing shale formations. *Energy Fuel* 32 (2), 1963–1978. doi:10.1021/acs.energyfuels.7b03074

Pan, Z., Connell, L. D., Camilleri, M., and Connelly, L. (2010). Effects of matrix moisture on gas diffusion and flow in coal. *Fuel* 89 (11), 3207–3217. doi:10.1016/j.fuel.2010.05.038

Perera, M. S. A., Ranjith, P. G., Choi, S. K., and Airey, D. (2011). The effects of sub-critical and super-critical carbon dioxide adsorption-induced coal matrix swelling on the permeability of naturally fractured black coal. *Energy* 36 (11), 6442–6450. doi:10.1016/j.energy.2011.09.023

Qu, S., Yang, J., and Liu, Z. (2012). CO_2 sorption on coals: Contribution of minerals and influence of supercritical CO_2 pre-exposure. *Energy Fuel.* 26 (6), 3928–3934. doi:10.1021/ef300123s

Song, Y., Zou, Q., Su, E., Zhang, Y., and Sun, Y. (2020). Changes in the microstructure of low-rank coal after supercritical CO_2 and water treatment. *Fuel* 279, 118493. doi:10.1016/j.fuel.2020.118493

Talapatra, A., and Karim, M. M. (2020). The influence of moisture content on coal deformation and coal permeability during coalbed methane (CBM) production in wet reservoirs. *J. Pet. Explor. Prod. Te.* 10 (5), 1907–1920. doi:10.1007/s13202-020-00880-x

Teng, T., Gao, F., Ju, Y., and Xue, Y. (2017). How moisture loss affects coal porosity and permeability during gas recovery in wet reservoirs? *Int. J. Min. Sci. Techno.* 27 (6), 899–906. doi:10.1016/j.ijmst.2017.06.016

Wang, H., Fu, X., Jian, K., Li, T., and Luo, P. (2015). Changes in coal pore structure and permeability during N_2 injection. *J. Nat. Gas. Sci. Eng.* 27, 1234–1241. doi:10.1016/j.jngse.2015.09.068

Wang, X., Zhang, D., Geng, J., Jin, Z., Wang, C., and Ren, K. (2022b). Effects of CO_2 intrusion on pore structure characteristics of mineral-bearing coal: Implication for CO_2 injection pressure. *J. Nat. Gas. Sci. Eng.* 108, 104808. doi:10.1016/j.jngse.2022.104808

Wang, Y., Guo, C., Du, C., Chen, X., Jia, L., Guo, X., et al. (2021a). Carbon peak and carbon neutrality in China: Goals, implementation path, and prospects. *China Geol.* 4 (0), 1–27. doi:10.31035/cg2021083

Wang, Z., Ge, Z., Li, R., Zhou, Z., Hou, Y., and Zhang, H. (2022a). Coupling effect of temperature, gas, and viscoelastic surfactant fracturing fluid on the chemical structure of deep coal: An experimental study. *Energy Fuel.* 36 (7), 3468–3480. doi:10.1021/acs.energyfuels.1c03796

Wang, Z., Ge, Z., Li, R., Zhou, Z., Hou, Y., and Zhang, H. (2021b). Coupling effect of temperature, gas, and viscoelastic surfactant fracturing fluid on the microstructure and its fractal characteristics of deep coal. *Energy Fuel.* 35 (23), 19423–19436. doi:10.1021/acs.energyfuels.1c02809

Xu, H., Zhu, S., and Shi, H. (2022). Is it possible to reduce agricultural carbon emissions through more efficient irrigation: Empirical evidence from China. *Water* 14 (8), 1218. doi:10.3390/w14081218

Yi, Z., Xiaomin, F., Xue, H., Zeyu, N., and Jun, X. (2012). Evaluation of coal bed methane content using BET adsorption isotherm equation. *Glob. Geol.* 15, 74–77. doi:10.3969/j.issn.1673-9736.2012.01.11

Zepeng, W., Zhaolong, G., Ruihui, L., Xianfeng, L., Haoming, W., and Shihui, G. (2022). Effects of acid-based fracturing fluids with variable hydrochloric acid contents on the microstructure of bituminous coal: An experimental study. *Energy* 244, 122621. doi:10.1016/j.energy.2021.122621

Zhang, G., Ranjith, P. G., Wu, B., Perera, M. S. A., Haque, A., and Li, D. (2019b). Synchrotron X-ray tomographic characterization of microstructural evolution in coal due to supercritical CO_2 injection at *in-situ* conditions. *Fuel* 255, 115696. doi:10.1016/j.fuel.2019.115696

Zhang, K., Cheng, Y., Li, W., Wu, D., and Liu, Z. (2017). Influence of supercritical CO_2 on pore structure and functional groups of coal: Implications for CO_2 sequestration. *J. Nat. Gas. Sci. Eng.* 40, 288–298. doi:10.1016/j.jngse.2017.02.031

Zhang, K., Sang, S., Liu, C., Ma, M., and Zhou, X. (2019c). Experimental study the influences of geochemical reaction on coal structure during the CO_2 geological storage in deep coal seam. *J. Pet. Sci. Eng.* 178, 1006–1017. doi:10.1016/j.petrol.2019.03.082

Zhang, S., Wu, C., and Liu, H. (2020). Comprehensive characteristics of pore structure and factors influencing micropore development in the Laochang mining area, eastern Yunnan, China. *J. Pet. Sci. Eng.* 190, 107090. doi:10.1016/j.petrol.2020.107090

Zhang, X., Wu, C., and Wang, Z. (2019a). Experimental study of the effective stress coefficient for coal permeability with different water saturations. *J. Pet. Sci. Eng.* 182, 106282. doi:10.1016/j.petrol.2019.106282